NUCLEAR EFFECTS IN (ANTI)NEUTRINO CHARGED-CURRENT QUASIELASTIC SCATTERING AT MINERνA KINEMATICS*

M.V. Ivanov[a], A.N. Antonov[a], G.D. Megias[b]
R. González-Jiménez[c], M.B. Barbaro[d], J.A. Caballero[b]
T.W. Donnelly[e], J.M. Udias[f]

[a]Institute for Nuclear Research and Nuclear Energy
Bulgarian Academy of Sciences, Sofia 1784, Bulgaria
[b]Departamento de Física Atómica, Molecular y Nuclear
Universidad de Sevilla, 41080 Sevilla, Spain
[c]Department of Physics and Astronomy, Ghent University
Proeftuinstraat 86, 9000 Gent, Belgium
[d]Dipartimento di Fisica, Università di Torino and INFN, Sezione di Torino
Via P. Giuria 1, 10125 Torino, Italy
[e]Center for Theoretical Physics
Laboratory for Nuclear Science and Department of Physics
Massachusetts Institute of Technology, Cambridge, Massachusetts 02139, USA
[f]Grupo de Física Nuclear, Departamento de Física Atómica, Molecular y Nuclear
Universidad Complutense de Madrid, CEI Moncloa, Madrid, Spain

We compare the characteristics of the charged-current quasielastic neutrino and antineutrino scattering obtained in two different nuclear models, the phenomenological SuperScaling Approximation and the model using a realistic spectral function $S(p, \mathcal{E})$ that gives a scaling function in accordance with the (e, e') scattering data, with the recent data published by the MINERνA Collaboration. The spectral function accounts for the nucleon–nucleon (NN) correlations by using natural orbitals from the Jastrow correlation method and has a realistic energy dependence. Both models provide a good description of the data without the need of an *ad hoc* increase of the value of the mass parameter in the axial-vector dipole form factor.

1. Introduction

The MINERνA Collaboration has recently measured differential cross sections for neutrino and antineutrino charged-current quasielastic (CCQE)

---

scattering on a hydrocarbon target [1,2]. "Quasielastic" events are defined, in this case, as containing no mesons in the final state. The beam energy goes from 1.5 to 10 GeV and is peaked at $E_\nu \sim 3.5$ GeV. At lower energies $E_\nu \sim 0.8$ GeV, the MiniBooNE experiment has reported [3] CCQE cross sections that are higher than most theoretical predictions based on the impulse approximation (IA), leading to the suggestion that non-QE processes induced by two-body currents may play a significant role in this energy domain [4–7]. These effects have sometimes been simulated, in the Relativistic Fermi Gas (RFG) framework, by a value of the nucleon axial-vector dipole mass $M_A = 1.35$ GeV [3], which is significantly larger than the standard value $M_A = 1.03$ GeV extracted from neutrino–deuterium quasielastic scattering. On the other hand, higher-energy data from the NOMAD experiment ($E_\nu \sim 3$–100 GeV) [8] are well-accounted for by IA models [9]. The MINERνA experiment is situated in between these two energy regions and its interpretation can, therefore, provide valuable information on the long-standing problem of assessing the role of correlations and meson exchange currents (MEC) in the nuclear dynamics [10–12].

In this paper, we present results corresponding to two different nuclear models: the SuSA (SuperScaling Approximation) and the model using a realistic spectral function $S(p, \mathcal{E})$. Both have been extensively tested against existing QE electron scattering data over a wide energy range. The detailed description of these models can be found in our previous work (see, *e.g.*, [13] and [14,15]). Here, we just summarize their main features.

2. Theoretical scheme and results

SuSA [13] is based on the idea of using electron scattering data to predict CC neutrino cross sections: a phenomenological "superscaling function" $f(\psi)$, depending only on one "scaling variable" $\psi(q, \omega)$ and embodying the essential nuclear dynamics, can be extracted from QE longitudinal (e, e') data within a fully relativistic framework. This function is then multiplied by the appropriate charge-changing $N \to N$ ($n \to p$ for neutrino and $p \to n$ for antineutrino scattering) weak interaction cross sections to obtain the various response functions that contribute to the inclusive neutrino–nucleus cross section [16]. On the one hand, the model gives a good representation of the purely nucleonic contributions to the existing QE electron scattering data, to the extent that the quasielastic scattering can be isolated. On the other hand, it does not account for the inelastic scattering and MEC which are mainly seen in the transverse channel. For the former, the SuSA approach has been successfully extended to higher energies into the non-QE regime where inelastic contributions dominate [17]. The latter have been modeled using extensions of the RFG for two-body operators and typically cause 10–20% scaling violations.

The second model we consider is the model using a realistic spectral function $S(p, \mathcal{E})$ that gives a scaling function in accordance with the (e, e') scattering data [14, 15]. Within the PWIA (see, *e.g.*, [14, 18] and details therein), the differential cross section for the $(e, e'N)$ process factorizes in the form of

$$\left[\frac{\mathrm{d}\sigma}{\mathrm{d}\epsilon' \, \mathrm{d}\Omega' \, \mathrm{d}p_N \, \mathrm{d}\Omega_N} \right]_{(e,e'N)}^{\mathrm{PWIA}} = K \sigma^{eN}(q, \omega; p, \mathcal{E}, \phi_N) S(p, \mathcal{E}), \qquad (2.1)$$

where σ^{eN} is the electron–nucleon cross section for a moving off-shell nucleon, K is a kinematical factor, and $S(p, \mathcal{E})$ is the spectral function giving the probability to find a nucleon of certain momentum and energy in the nucleus. In Eq. (2.1), p is the missing momentum and $\mathcal{E}$ is the excitation energy of the residual system. The scaling function can be represented in the form of

$$F(q, \omega) \cong \frac{[\mathrm{d}\sigma/\mathrm{d}\epsilon' \, \mathrm{d}\Omega']_{(e,e')}}{\bar{\sigma}^{eN}(q, \omega; p = |y|, \mathcal{E} = 0)}, \qquad (2.2)$$

where the electron–single nucleon cross section $\bar{\sigma}^{eN}$ is taken at $p = |y|$, y being the smallest possible value of p in electron–nucleus scattering for the smallest possible value of the excitation energy ($\mathcal{E} = 0$). The theoretical concept of superscaling has been introduced within the relativistic Fermi gas (RFG) model [19, 20]. In the RFG model, the scaling function $f_{\mathrm{RFG}}(\psi') = k_{\mathrm{F}} F$ has the form [21]

$$f_{\mathrm{RFG}}(\psi') \simeq \tfrac{3}{4} \left(1 - \psi'^2 \right) \theta \left(1 - \psi'^2 \right). \qquad (2.3)$$

As pointed out in [21], however, the actual dynamical physical reason of the superscaling is more complex than that provided by the RFG model.

In Ref. [14], more information about the spectral function was extracted within PWIA from the experimentally known scaling function. It contains effects beyond the mean-field approximation leading to a realistic energy dependence and accounts for short-range NN correlations. It is written in the form of

$$S(p, \mathcal{E}) = \sum_i 2(2j_i + 1) n_i(p) L_{\Gamma_i}(\mathcal{E} - \mathcal{E}_i), \qquad (2.4)$$

where the Lorentzian function is used

$$L_{\Gamma_i}(\mathcal{E} - \mathcal{E}_i) = \frac{1}{\pi} \frac{\Gamma_i/2}{(\mathcal{E} - \mathcal{E}_i)^2 + (\Gamma_i/2)^2} \qquad (2.5)$$

with Γ_i being the width of a given s.p. hole state. In the calculations, we used the values $\Gamma_{1p} = 6$ MeV and $\Gamma_{1s} = 20$ MeV, which are fixed to

the experimental widths of the $1p$ and $1s$ states in ^{12}C [22]. In Eq. (2.4), the s.p. momentum distributions $n_i(p)$ were taken firstly to correspond to harmonic-oscillator (HO) shell-model s.p. wave functions, and second, to natural orbitals (NOs) s.p. wave functions $\varphi_\alpha(\boldsymbol{r})$ defined in [23] as the complete orthonormal set of s.p. wave functions that diagonalize the one-body density matrix $\rho(\boldsymbol{r}, \boldsymbol{r}')$

$$\rho\left(\boldsymbol{r}, \boldsymbol{r}'\right) = \sum_\alpha N_\alpha \varphi_\alpha^*(\boldsymbol{r}) \varphi_\alpha\left(\boldsymbol{r}'\right) , \tag{2.6}$$

where the eigenvalues N_α $(0 \leq N_\alpha \leq 1, \sum_\alpha N_\alpha = A)$ are the natural occupation numbers. In [14], we used $\rho(\boldsymbol{r}, \boldsymbol{r}')$ obtained within the lowest-order approximation of the Jastrow correlation methods [24]. The realistic spectral function $S(p, \mathcal{E})$ is presented in Fig. 1, where the two shells $1p$ and $1s$ are clearly visible.
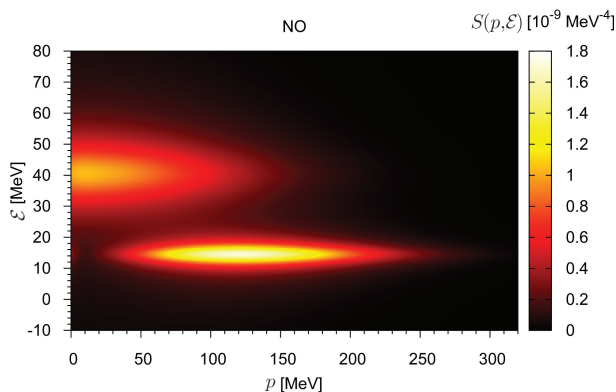

Fig. 1. The ^{12}C realistic spectral function $S(p, \mathcal{E})$, which is constructed using natural orbital single-particle momentum distributions from the Jastrow correlation method and Lorentzian function for the energy dependence.

For accounting for the FSI, we follow the approach given in Ref. [25] concerning two types of FSI effects, the Pauli blocking and the interaction of the struck nucleon with the spectator system by means of the time-independent optical potential (OP) $U = V - \imath W$. The latter can be accounted for [26] by replacing in the PWIA expression for the inclusive electron–nucleus scattering cross section

$$\frac{d\sigma_t}{d\omega\, d|\boldsymbol{q}|} = 2\pi\alpha^2 \frac{|\boldsymbol{q}|}{E_{\boldsymbol{k}}^2} \int dE\, d^3p\, \frac{S_t(\boldsymbol{p}, E)}{E_{\boldsymbol{p}} E_{\boldsymbol{p}'}} \delta\left(\omega + M - E - E_{\boldsymbol{p}'}\right) L_{\mu\nu}^{\text{em}} H_{\text{em},t}^{\mu\nu} \tag{2.7}$$

the energy-conserving delta function by

$$\delta\left(\omega + M - E - E_{\boldsymbol{p}'}\right) \to \frac{W/\pi}{W^2 + [\omega + M - E - E_{\boldsymbol{p}'} - V]^2} . \tag{2.8}$$

In Eq. (2.7), the index t denotes the nucleon isospin, $L_{\mu\nu}^{\text{em}}$ and $H_{\text{em},t}^{\mu\nu}$ are the leptonic and hadronic tensors, respectively, and $S_t(\boldsymbol{p}, E)$ is the proton (neutron) spectral function. The real (V) and imaginary (W) parts of the OP in (2.7) and (2.8) are obtained in Ref. [27] from the Dirac OP.

The CC (anti)neutrino cross section in the target laboratory frame is given in the form of (see for details [13, 28])

$$\left[\frac{\mathrm{d}^2\sigma}{\mathrm{d}\Omega\,\mathrm{d}k'}\right]_\chi \equiv \sigma_0 \mathcal{F}_\chi^2, \tag{2.9}$$

where $\chi = +$ for neutrino-induced reaction (*e.g.*, $\nu_\ell + n \to \ell^- + p$, where $\ell = e, \mu, \tau$) and $\chi = -$ for antineutrino-induced reactions (*e.g.*, $\bar{\nu}_\ell + p \to \ell^+ + n$). The quantity $\mathcal{F}_\chi^2$ in (2.9) depends on the nuclear structure and is presented [13] as a generalized Rosenbluth decomposition containing leptonic factors and five nuclear response functions, namely charge–charge (CC), charge–longitudinal (CL), longitudinal–longitudinal (LL), vector–transverse (T) and axial–transverse (T') expressed by the nuclear tensor and the scaling function.

To obtain the scaling function, we use the spectral function $S(p, \mathcal{E})$ from (2.4) with $n_i(p)$ corresponding to HO or NOs s.p. wave functions, and the Lorentzian function (2.5). We calculate the electron-^{12}C cross section by using Eqs. (2.7) and (2.8), and the scaling function $F(q, \omega)$ within the PWIA from Eq. (2.2). By multiplying $F(q, \omega)$ by k_{F}, the scaling function $f(\psi')$ is obtained. In this way, the results (Fig. 2) for the HO+FSI (dashed line) and NO+FSI (dash-dotted line) are obtained. As a reference, there are also shown the scaling functions in the cases of SuSA (dotted line) and RFG (solid line). The accounting for FSI leads to a small asymmetry of the scaling func-
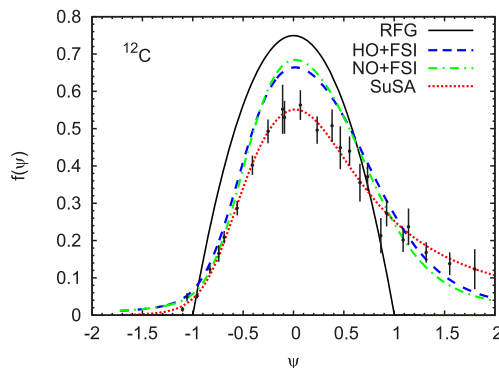

Fig. 2. Results for the scaling function $f(\psi)$ for ^{12}C obtained using HO+FSI and NO+FSI approaches are compared with the RFG and SuSA results, as well as with the longitudinal experimental data.

tion. Moreover, we found that the asymmetry in the scaling function gets larger by using the Lorentzian function [Eq. (2.5)] for the energy dependence of the spectral function than by using the Gaussian function [14, 15].

The results for the total cross sections obtained in [15] within the HO+FSI and NO+FSI are given in Fig. 3 and compared with the SuSA and RFG results and the MiniBooNE [3] and NOMAD [8] data (up to 100 GeV). All models give results that agree with the NOMAD data but underpredict the MiniBooNE ones, more seriously in the ν_μ than in $\bar\nu_\mu$ cases. The discrepancy with the MiniBooNE data (at energies < 1 GeV) is most likely due to missing effects beyond the IA, *e.g.* those of the $2p$–$2h$ excitations that have contributions in the transverse responses. This concerns also the similar disagreement that appears when the phenomenological scaling function in SuSA is used. The latter, being exctracted from the (e, e') data, is a purely longitudinal QE response and thus is nearly insensitive to $2p$–$2h$ MEC contributions.
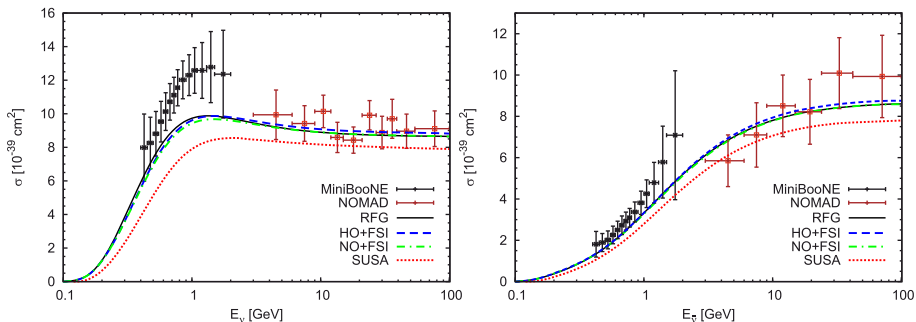

Fig. 3. (Left panel) CCQE ν_μ+^{12}C total cross sections per nucleon displayed *versus* neutrino energy E_ν evaluated using the RFG, HO+FSI, NO+FSI, and SuSA approaches with the standard value of the axial-vector dipole mass $M_A = 1.03 \text{ GeV}/c^2$ are compared with the MiniBooNE [3] and NOMAD [8] experimental data. (Right panel) CCQE $\bar\nu_\mu$+^{12}C total cross section.

In Fig. 4, we display the flux-folded differential cross section $d\sigma/dQ^2_{\text{QE}}$ for both neutrino (left panel) and antineutrino (right panel) scattering off a hydrocarbon (CH) target as a function of the reconstructed four-momentum transfer squared (Q^2_{QE}) that is obtained in the same way as for the experiment, assuming an initial-state nucleon at rest with a constant binding energy, E_b, set to 34 MeV (30 MeV) in the neutrino (antineutrino) case. The cross sections are folded with the MINERνA ν_μ and $\bar\nu_\mu$ fluxes [1, 2], and the nucleon's axial mass has the standard value $M_A = 1.03$ GeV. We observe that RFG, SuSA, HO+FSI and NO+FSI approache yield predictions in an excellent agreement with the experimental data, leaving not much space

for large effects of $2p$–$2h$ contributions. HO+FSI and NO+FSI results are higher than the SuSA ones and lie closer to the RFG results. In the RFG calculation, we use the formalism of [19], assuming a Fermi momentum of 228 MeV/c and an energy shift of 20 MeV. Note that the RFG model with the standard value of the axial mass (solid curve) also fits the data, being in a very good agreement with the other approaches. Finally, the spread in the curves corresponding to the four models is less than 7% in the case of neutrinos and less than 5% in the case of antineutrinos.
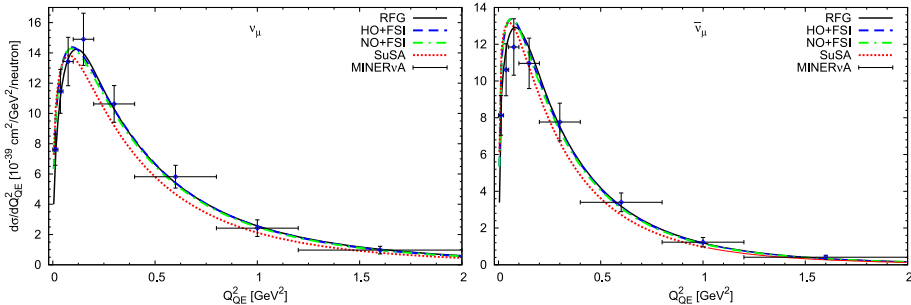

Fig. 4. Flux-folded CCQE $\nu_\mu + {}^{12}$C (left panel) and $\bar{\nu}_\mu + {}^{12}$C (right panel) scattering cross section per target nucleon as a function of Q^2_{QE} and evaluated in the SuSA, RFG, HO+FSI, and NO+FSI models; data [1,2].

3. Conclusions

1. The results with different spectral functions (HO and NO) give quite similar results (within 5–7%) for the CCQE cross sections, signaling that the process is not too sensitive to the specific treatment of the bound state.

2. The FSI leads to an increase of about 2% using spectral functions with HO and NO s.p. wave functions, almost independently of the neutrino energy.

3. All approaches based on IA underestimate MiniBooNE data for the flux-averaged CCQE ($\nu_\mu(\bar{\nu}_\mu) + {}^{12}$C) differential cross sections and the total cross section although the shape of the cross section is represented by NO+FSI and HO+FSI approaches. For $\bar{\nu}$, the agreement is much better.

4. All models give results that are compatible with the MINERνA and NOMAD data. This points to the importance of the evaluation of non-impulsive contributions, like those associated to MEC and their evolution with energy. The $2p$–$2h$ contributions may be responsible for the observed discrepancy in our analyses. Similar disagreement is observed for the phenomenological scaling function of SuSA, that is

purely longitudinal QE response and *2p–2h MEC should not contribute to it when properly extracted from QE electron scattering, but could contribute to QE neutrino scattering because of the axial current.*

REFERENCES

[1] G.A. Fiorentini *et al.* [MINERνA Collaboration], *Phys. Rev. Lett.* **111**, 022502 (2013).

[2] L. Fields *et al.* [MINERνA Collaboration], *Phys. Rev. Lett.* **111**, 022501 (2013).

[3] A.A. Aguilar-Arevalo *et al.* [MiniBooNE Collaboration], *Phys. Rev. D* **81**, 092005 (2010); **88**, 032001 (2013).

[4] M. Martini *et al.*, *Phys. Rev. C* **81**, 045502 (2010).

[5] J.E. Amaro *et al.*, *Phys. Lett. B* **696**, 151 (2011).

[6] J.E. Amaro *et al.*, *Phys. Rev. Lett.* **108**, 152501 (2012).

[7] J. Nieves *et al.*, *Phys. Lett. B* **707**, 72 (2012).

[8] V. Lyubushkin *et al.*, *Eur. Phys. J. C* **63**, 355 (2009).

[9] G.D. Megias *et al.*, *Phys. Lett. B* **725**, 170 (2013).

[10] T.W. Donnelly *et al.*, *Phys. Lett. B* **76**, 393 (1978).

[11] A. De Pace *et al.*, *Nucl. Phys. A* **726**, 303 (2003).

[12] J.E. Amaro *et al.*, *Phys. Rev. C* **82**, 044601 (2010).

[13] J.E. Amaro *et al.*, *Phys. Rev. C* **71**, 015501 (2005).

[14] A.N. Antonov *et al.*, *Phys. Rev. C* **83**, 045504 (2011).

[15] M.V. Ivanov *et al.*, *Phys. Rev. C* **89**, 014607 (2014); **91**, 034607 (2015).

[16] G.D. Megias *et al.*, *Phys. Rev. D* **89**, 093002 (2014) [*Erratum ibid.* **91**, 039903 (2015)].

[17] C. Maieron *et al.*, *Phys. Rev. C* **80**, 035504 (2009).

[18] J.A. Caballero *et al.*, *Phys. Rev. C* **81**, 055502 (2010).

[19] W.M. Alberico *et al.*, *Phys. Rev. C* **38**, 1801 (1988).

[20] M.B. Barbaro *et al.*, *Nucl. Phys. A* **643**, 137 (1998).

[21] T.W. Donnelly, I. Sick, *Phys. Rev. C* **60**, 065502 (1999).

[22] D. Dutta, Ph.D. Thesis, Northwestern University, 1999.

[23] P.-O. Löwdin, *Phys. Rev.* **97**, 1474 (1955).

[24] M.V. Stoitsov, A.N. Antonov, S.S. Dimitrova, *Phys. Rev. C* **48**, 74 (1993).

[25] A.M. Ankowski, J.T. Sobczyk, *Phys. Rev. C* **77**, 044311 (2008).

[26] Y. Horikawa, F. Lenz, N.C. Mukhopadhyay, *Phys. Rev. C* **22**, 1680 (1980).

[27] E.D. Cooper *et al.*, *Phys. Rev. C* **47**, 297 (1993).

[28] A.N. Antonov *et al.*, *Phys. Rev. C* **74**, 054603 (2006).